



UNIVERSITI PUTRA MALAYSIA

**PREPARATION AND CHARACTERISATION OF NEW OXIDE ION
CONDUCTORS IN THE $\text{Bi}_2\text{-(W, Mo)-O}_6$ SYSTEM**

SIM LENG TZE

FSAS 2000 37

**PREPARATION AND CHARACTERISATION OF NEW OXIDE ION
CONDUCTORS IN THE $\text{Bi}_2\text{-(W, Mo)-O}_6$ SYSTEM**

By

SIM LENG TZE

**Thesis Submitted in Fulfilment of the Requirements for the Degree of Master
of Science in the Faculty of Science and Environmental Studies
Universiti Putra Malaysia**

December 2000



For my parents, with love



Abstract of thesis presented to the Senate of Universiti Putra Malaysia in fulfilment of the requirement for the degree of Master of Science

PREPARATION AND CHARACTERISATION OF NEW OXIDE ION CONDUCTORS IN THE $\text{Bi}_2\text{-(W, Mo)-O}_6$ SYSTEM

By

SIM LENG TZE

December 2000

Chairperson: Professor Lee Chnoong Kheng, Ph.D.

Faculty: Science and Environmental Studies

Bi_2WO_6 , Bi_2MoO_6 and their related materials were prepared by solid state reactions. The phase purity of the materials was determined by X-ray diffraction (XRD). Further characterisation using Fourier-transform infrared (FT-IR) spectroscopy, differential thermal analysis (DTA) and impedance spectroscopy were carried out on single phase materials. Thermogravimetric analysis (TGA) and scanning electron microscopy (SEM) were also performed on selected samples.

Only Nb and Ta could be introduced as dopant into Bi_2WO_6 with rather limited solid solution formation while introduction of dopants other than W into $\gamma\text{-Bi}_2\text{MoO}_6$ was unsuccessful. From results obtained in IR and DTA studies, it appears that the metal-oxygen bondings in Nb- and Ta-doped materials are weaker as compared to those in the parent material, Bi_2WO_6 . The conductivity of these materials was about two orders of magnitude higher than that of Bi_2WO_6 . Introduction of lower valency cation results in the creation of oxygen vacancies resulting in higher conductivity.

The IR and XRD patterns of both γ - Bi_2WO_6 and γ - Bi_2MoO_6 are very similar since the materials are isostructural.

Complete solid solutions in the γ - Bi_2WO_6 - γ - Bi_2MoO_6 system were obtained when prepared via low temperature route. This was made possible since the Hume-Rothery rules were fully obeyed by these materials. However, some of these materials were metastable and decomposed into mixed phases upon heating at higher temperatures. Generally, the conductivity in the system was comparable.

The conductivity of γ' - Bi_2MoO_6 is very dependent on sintering temperature and time. It is possible that loss of oxygen occurs upon sintering at elevated temperatures leading to the formation of non-stoichiometric γ' - $\text{Bi}_2\text{MoO}_{6-\delta}$. From ac impedance studies, oxide ions appear to be the main charge carriers in this material.

Phase diagram in the Bi_2WO_6 - Bi_2MoO_6 system was constructed based on results obtained from different heating experiments, XRD and DTA results.

Abstrak tesis yang dikemukakan kepada Senat Universiti Putra Malaysia sebagai memenuhi keperluan untuk ijazah Master Sains

**PENYEDIAAN AND PENCIRIAN KONDUKTOR ION OKSIDA BARU
DALAM SISTEM $\text{Bi}_2\text{-(W, Mo)-O}_6$**

Oleh

SIM LENG TZE

Disember 2000

Pengerusi: Professor Lee Chnoong Kheng, Ph.D.

Fakulti: Sains dan Pengajian Alam Sekitar

Bi_2WO_6 , Bi_2MoO_6 dan bahan yang berkaitan telah disediakan melalui tindak balas keadaan pepejal. Ketulenan fasa bahan tersebut ditentukan dengan menggunakan pembelauan serbuk sinar-X (XRD). Teknik pencirian lanjutan menggunakan spektrometer inframerah transformasi Fourier (FT-IR), analisis pembezaan terma (DTA) dan spektroskopi impedans telah dijalankan ke atas sampel yang berfasa tunggal. Analisis termogravimetri (TGA) dan mikroskopi imbasan elektron (SEM) juga dijalankan ke atas sampel-sampel terpilih.

Hanya Nb dan Ta dapat diperkenalkan sebagai dopan ke dalam Bi_2WO_6 dengan pembentukan larutan pepejal yang agak terhad manakala dopan selain daripada W gagal diperkenalkan ke dalam $\gamma\text{-Bi}_2\text{MoO}_6$. Keputusan yang diperolehi daripada IR dan DTA menunjukkan bahawa ikatan logam-oksigen adalah lebih lemah dalam bahan-bahan yang didopkan dengan Nb dan Ta berbanding dengan dalam Bi_2WO_6 . Kekonduksian bahan tersebut adalah lebih kurang dua tertib magnitud lebih tinggi

daripada Bi_2WO_6 . Pengaliran kation bervalensi lebih rendah membawa kepada penghasilan kekosongan tapak oksigen yang membawa kepada kekonduksian yang lebih tinggi.

Pola spektrum IR dan XRD bagi kedua-dua $\gamma\text{-Bi}_2\text{WO}_6$ dan $\gamma\text{-Bi}_2\text{MoO}_6$ adalah serupa kerana kedua-duanya memiliki struktur yang serupa.

Larutan pepejal yang lengkap diperolehi dalam sistem $\gamma\text{-Bi}_2\text{WO}_6$ - $\gamma\text{-Bi}_2\text{MoO}_6$ apabila disediakan pada suhu rendah. Ini adalah mungkin memandangkan kesemua petua Hume-Rothery dipatuhi oleh bahan tersebut. Akan tetapi, sesetengah bahan tersebut adalah metastabil dan terurai kepada fasa tercampur apabila dipanaskan pada suhu yang lebih tinggi. Secara amnya, kekonduksian bahan dalam sistem tersebut adalah lebih kurang sama.

Kekonduksian $\gamma\text{-Bi}_2\text{MoO}_6$ adalah sangat bergantung kepada suhu dan jangka masa pemanasan. Ada kemungkinan bahawa kehilangan oksigen berlaku semasa pemanasan pada suhu yang tinggi dan membawa kepada bahan tidak stoikiometri, $\gamma\text{-Bi}_2\text{MoO}_{6-\delta}$. Daripada ujikaji dengan impedans ac, ion oksida merupakan pembawa cas yang utama bagi bahan tersebut.

Gambarajah fasa dalam sistem Bi_2WO_6 - Bi_2MoO_6 telah dibina berdasarkan kepada keputusan yang diperolehi daripada ujikaji pemanasan yang berbeza, XRD dan DTA.

ACKNOWLEDGEMENTS

The author would like to express her deepest appreciation to Professor Dr Lee Chnoong Kheng for her invaluable assistance, dedication, guidance, patience, understanding and support throughout the project.

The author would also like to extend her gratitude to Professor Dr Abdul Halim Shaari and Associate Professor Dr Mansor Hashim of UPM for their invaluable suggestion, advice and fruitful discussion for without which, this thesis would not be completed.

In addition, the author would also like to thank the laboratory assistants and technicians, Mr Nordin Ismail, Mdm Rusnani Amirudin (FT-IR), Mr Kamal Margona (TGA, DTA) of Chemistry department, Mr Ho Oi Kuan, Ms Azilah Ab. Jalil, Mdm Faridah Akmal Ismail and Cik Sulaika (SEM) of Institute Bioscience, UPM who had assisted the author in the respective analytical area, for without them, this project would not be completed.

The author would also like to give her heart-felt thanks to her parents, her brother and sisters as well as her eldest brother-in-law for their continuous support and encouragement.

TABLE OF CONTENTS

	Page
DEDICATION	ii
ABSTRACT	iii
ABSTRAK	v
ACKNOWLEDGEMENTS	vii
APPROVAL SHEETS	viii
DECLARATION FORM	x
LIST OF TABLES	xiii
LIST OF FIGURES	xiv
LIST OF ABBREVIATIONS	xx
CHAPTER	
1 INTRODUCTION	1.1
1.1 Solid Electrolytes and Oxide Ion Conductors	1.1
1.1.1 Ionic Conduction	1.3
1.1.2 Oxygen Sensors	1.4
1.1.3 Solid Oxide Fuel Cells (SOFC's)	1.6
1.2 Objectives	1.9
2 LITERATURE REVIEW	
2.1 Oxide Ion Conductors	2.1
2.2 Bi ₂ WO ₆	2.4
2.2.1 Synthesis Conditions	2.4
2.2.2 Polymorphism	2.5
2.2.3 Structure of Bi ₂ WO ₆	2.7
2.2.4 Introduction of Dopant	2.12
2.3 Bi ₂ MoO ₆	2.14
2.3.1 Synthesis Conditions	2.14
2.3.2 Polymorphism	2.16
2.3.3 Structure of Bi ₂ MoO ₆	2.19
3 MATERIALS AND METHODS	
3.1 Synthesis	3.1
3.1.1 Bi ₂ WO ₆ Solid Solutions	3.1
3.1.2 γ'-Bi ₂ MoO ₆ Solid Solutions	3.3
3.1.3 γ-Bi ₂ MoO ₆ Solid Solutions	3.3
3.2 Analysis and Characterisation	3.4
3.2.1 Phase Purity – X-ray Diffraction (XRD)	3.4
3.2.2 Electrical Properties	3.4
3.2.3 Scanning Electron Microscopy (SEM)	3.15
3.2.4 Fourier-transform Infrared Spectroscopy (FT-IR)	3.15

3.2.5 Thermal Analysis	3.16
3.3 Phase Diagram	3.18
3.3.1 Melting Point	3.18
3.3.2 Phase Stability	3.18
3.4 Error Estimate	3.19
4 RESULTS AND DISCUSSION	4.1
4.1 Bi ₂ WO ₆ Solid Solutions	4.1
4.1.1 Phase Purity	4.1
4.1.2 Fourier-transform Infrared (FT-IR) Spectroscopy Analysis	4.17
4.1.3 Thermal Analysis	4.25
4.1.4 Electrical Properties	4.31
4.2 γ'-Bi ₂ MoO ₆ Solid Solutions	4.47
4.2.1 Phase Purity	4.47
4.2.2 Fourier-transform Infrared (FT-IR) Spectroscopy Analysis	4.55
4.2.3 Thermal Analysis	4.57
4.2.4 Electrical Properties	4.62
4.3 γ-Bi ₂ MoO ₆ Solid Solutions	4.85
4.3.1 Phase Purity	4.85
4.3.2 Fourier-transform Infrared (FT-IR) Spectroscopy Analysis	4.88
4.3.3 Thermal Analysis	4.92
4.3.4 Electrical Properties	4.94
4.4 Bi ₂ WO ₆ - Bi ₂ MoO ₆ Solid Solutions	4.99
4.4.1 Phase Purity	4.99
4.4.2 Fourier-transform Infrared (FT-IR) Spectroscopy Analysis	4.107
4.4.3 Thermal Analysis and Phase Diagram	4.107
4.4.4 Electrical Properties	4.119
5 CONCLUSION	5.1
REFERENCES/BIBLIOGRAPHY	R.1
APPENDICES	A.1
BIODATA OF AUTHOR	B.1

LIST OF TABLES

Table	Page
2.1 A summary of the three major displacive modes (Withers et al., 1991)	2.9
3.1 Capacitance values and their possible interpretation	3.10
3.2 Error estimate on experimental parameters	3.19
4.1 Results of doping experiments on phase purity of $\text{Bi}_2\text{W}_{1-x}\text{M}^*_x\text{O}_8$	4.5
4.2 Vibrational spectra of Bi_2WO_6 (values in cm^{-1}) and assignment of the internal modes	4.21
4.3 Phase transition temperatures of $\text{Bi}_2\text{W}_{1-x}\text{M}^*_x\text{O}_{6-x/2}$ solid solutions	4.28
4.4 Activation energy (E_a) and conductivity, σ of $\text{Bi}_2\text{W}_{1-x}\text{M}^*_x\text{O}_{6-x/2}$ solid solutions (1 st cooling cycle)	4.42
4.5 Results of doping experiments on phase purity of $\text{Bi}_2\text{Mo}_{1-x}\text{M}^*_x\text{O}_8$	4.49
4.6 Weight loss of γ' - Bi_2MoO_6 (prepared at 680°C) corresponding to prolonged heat treatment	4.57
4.7 Weight loss of γ' - Bi_2MoO_6 (prepared at 680°C) corresponding to prolonged heat treatment at 800°C	4.59
4.8 Effect of cooling process on weight loss of γ' - Bi_2MoO_6 (prepared at 680°C)	4.59
4.9 Activation energy of γ' - Bi_2MoO_6 calculated from the slope of the Arrhenius plots	4.71
4.10 Capacitance at Z''_{max} of the 1 st heating and the subsequent cooling cycles of γ' - Bi_2MoO_6 (1 st pellet) at 550°C and 800°C	4.84
4.11 Capacitance and the permittivity at Z''_{max} of γ' - Bi_2MoO_6 (1 st pellet) taken at the 11 th cooling cycle	4.84
4.12a Impedance data of γ - Bi_2MoO_6 in the 1 st heating cycle	4.100
4.12b Impedance data of γ - Bi_2MoO_6 in the 2 nd heating cycle	4.100
4.13 Synthesis temperatures of γ - $\text{Bi}_2\text{W}_{1-x}\text{Mo}_x\text{O}_6$ solid solutions	4.103
4.14 Thermal analysis of $\text{Bi}_2\text{W}_{1-x}\text{Mo}_x\text{O}_6$ solid solutions	4.111

LIST OF FIGURES

Figure		Page
1.1	Electrical conductivities of selected common substances and representative solid electrolytes (Greenblatt, 1994)	1.2
1.2	Schematic diagram showing main elements of a solid electrolyte oxygen concentration cell (Kocache, 1987)	1.5
1.3	Concept diagram of SOFC (Fisher, 1999)	1.7
2.1	Summary of phase transitions (Watanabe, 1982)	2.6
2.2	(a) Prototype structure of Bi_2WO_6 (Yonovskii and Voronkova, 1986) and (b) structure of Bi_2WO_6 (Islam et al., 1998)	2.8
2.3	Schematic representation of the atomic displacement patterns for the major displacive modes having (a) $F2mm$, (b) $Bmab$ and (c) $Abam$ symmetry (Thompson et al., 1992)	2.11
2.4	Phase transitions observed by Erman and Gal'perin (1971)	2.16
2.5	Phase transitions of Bi_2MoO_6 (Watanabe and Kodama, 1980)	2.17
2.6	Phase transitions of Bi_2MoO_6 (Kodama and Watanabe, 1985)	2.18
3.1	Flow chart for the preparation of bismuth tungstate solid solutions	3.2
3.2	Flow chart for the preparation of high temperature form of bismuth molybdate solid solutions	3.3
3.3	Admittance bridge	3.5
3.4	Impedance bridge	3.5
3.5	Semi-circle and spike in a complex Z^* plot	3.8
3.6	Semi-circles in a complex Z^* plot	3.9
3.7	Brickwork model of grain and grain boundary regions in a ceramic placed between metal electrodes (Irvine et al., 1990)	3.9
3.8	Impedance diagram due to a blocking interface: (a) a perfectly smooth interface; (b) rough electrode or due to Warburg impedance (Armstrong and Todd, 1995)	3.12

3.9	(a) A complex Z^* plot and (b) the respective Z'' and M'' spectroscopic plots	3.13
4.1	XRD pattern of Bi_2WO_6	4.2
4.2	Comparison of XRD pattern with JCPDS using μPDSM : (a) Bi_2WO_6 and (b) JCPDS card number 39-0256	4.3
4.3	XRD patterns of $\text{Bi}_2\text{W}_{1-x}\text{Nb}_x\text{O}_8$: (a) $x=0.05$, (b) $x=0.10$, (c) $x=0.15$, (d) $x=0.20$, (e) $x=0.25$, (f) $x=0.30$, (g) $x=0.40$ and (h) $x=0.50$	4.6
4.4	XRD patterns of $\text{Bi}_2\text{W}_{1-x}\text{Nb}_x\text{O}_8$: (a) $x=0.20$, (b) $x=0.25$, (c) $x=0.30$, (d) $x=0.40$ and (e) $x=0.50$	4.7
4.5	XRD patterns of $\text{Bi}_2\text{W}_{1-x}\text{Ta}_x\text{O}_8$: (a) $x=0.05$, (b) $x=0.10$, (c) $x=0.15$, (d) $x=0.20$, (e) $x=0.25$, (f) $x=0.30$ and (g) $x=0.50$	4.8
4.6	XRD patterns of $\text{Bi}_2\text{W}_{1-x}\text{Ta}_x\text{O}_8$: (a) $x=0.20$, (b) $x=0.25$, (c) $x=0.30$ and (d) $x=0.50$	4.9
4.7	XRD patterns of (a) $\text{Bi}_2\text{W}_{1-x}\text{Nb}_x\text{O}_8$ and (b) $\text{Bi}_2\text{W}_{1-x}\text{Ta}_x\text{O}_8$	4.11
4.8	XRD patterns of $\text{Bi}_2\text{W}_{1-x}\text{V}_x\text{O}_8$: (a) $x=0.05$, (b) $x=0.10$, (c) $x=0.15$ and (d) $x=0.20$	4.12
4.9	XRD patterns of $\text{Bi}_2\text{W}_{1-x}\text{P}_x\text{O}_8$: (a) $x=0.05$, (b) $x=0.10$ and (c) $x=0.15$	4.13
4.10	XRD patterns of $\text{Bi}_2\text{W}_{1-x}\text{As}_x\text{O}_8$: (a) $x=0.05$ and (b) $x=0.10$	4.15
4.11	XRD patterns of $\text{Bi}_2\text{W}_{1-x}\text{Sb}_x\text{O}_8$: (a) $x=0.05$ and (b) $x=0.10$	4.16
4.12	IR spectrum of Bi_2WO_6 showing (a) the whole spectrum and (b) the far IR region	4.18
4.13	IR spectrum of blank KBr run in ambient atmosphere	4.19
4.14	IR spectra of $\text{Bi}_2\text{W}_{1-x}\text{Nb}_x\text{O}_{6-x/2}$ solid solutions: (a) $x=0$, (b) $x=0.05$, (c) $x=0.10$, (d) $x=0.15$ and (e) $x=0.20$	4.23
4.15	IR spectra of $\text{Bi}_2\text{W}_{1-x}\text{Ta}_x\text{O}_{6-x/2}$ solid solutions: (a) $x=0$, (b) $x=0.05$, (c) $x=0.10$, (d) $x=0.15$ and (e) $x=0.20$	4.24
4.16	DTA thermograms of Bi_2WO_6 at heating rate of (a) $10^\circ\text{C}/\text{min}$, (b) $20^\circ\text{C}/\text{min}$ and (c) $30^\circ\text{C}/\text{min}$	4.26

4.17	DTA thermograms of $\text{Bi}_2\text{W}_{1-x}\text{Nb}_x\text{O}_{6-x/2}$ solid solutions: (a) $x=0$, (b) $x=0.10$, (c) $x=0.15$ and (d) $x=0.20$	4.29
4.18	DTA thermograms of $\text{Bi}_2\text{W}_{1-x}\text{Ta}_x\text{O}_{6-x/2}$ solid solutions: (a) $x=0$, (b) $x=0.10$, (c) $x=0.15$ and (d) $x=0.20$	4.30
4.19	Complex plane plots of Bi_2WO_6 at (a) 351°C and (b) 550°C	4.32
4.20	Arrhenius plot of Bi_2WO_6	4.34
4.21	Complex plane plots of Bi_2WO_6 (sintered at 900°C) at (a) 350°C , (b) 500°C and (c) 800°C	4.35
4.22	Modulus plots of Bi_2WO_6 at various temperatures (1 st heating cycle)	4.38
4.23	Complex plane plots of $\text{Bi}_2\text{W}_{0.95}\text{Nb}_{0.05}\text{O}_{5.975}$ at (a) 300°C and (b) 400°C	4.40
4.24	Complex plane plot of $\text{Bi}_2\text{W}_{0.95}\text{Nb}_{0.05}\text{O}_{5.975}$ at 400°C	4.41
4.25	Arrhenius plots of $\text{Bi}_2\text{W}_{1-x}(\text{Nb},\text{Ta})_x\text{O}_{6-x/2}$	4.43
4.26	Arrhenius plots of $\text{Bi}_2\text{W}_{1-x}\text{Nb}_x\text{O}_{6-x/2}$ solid solutions	4.45
4.27	Arrhenius plots of $\text{Bi}_2\text{W}_{1-x}\text{Ta}_x\text{O}_{6-x/2}$ solid solutions	4.46
4.28	XRD pattern of γ' - Bi_2MoO_6	4.48
4.29	XRD patterns of γ' - $\text{Bi}_2\text{Mo}_{1-x}\text{V}_x\text{O}_8$: (a) $x=0.05$ (42 hours at 800°C), (b) $x=0.05$ (64 hours at 800°C) and (c) $x=0.10$ (22 hours at 900°C)	4.51
4.30	XRD patterns of γ' - $\text{Bi}_2\text{Mo}_{1-x}\text{As}_x\text{O}_8$: (a) $x=0.05$ (44 hours at 800°C), (b) $x=0.05$ (22 hours at 850°C) and (c) $x=0.10$ (22 hours at 850°C)	4.52
4.31	XRD patterns of γ' - $\text{Bi}_2\text{Mo}_{1-x}\text{M}^*_x\text{O}_8$: (a) $\text{M}^*=\text{Ti}$, (b) $\text{M}^*=\text{Sb}$ and (c) $\text{M}^*=\text{Zr}$	4.53
4.32	XRD patterns of γ' - $\text{Bi}_2\text{Mo}_{1-x}\text{M}^*_x\text{O}_8$: (a) $\text{M}^*=\text{Nb}$ and (b) $\text{M}^*=\text{Ta}$	4.54
4.33	IR spectrum of γ' - Bi_2MoO_6 showing (a) the whole spectrum and (b) the far IR region	4.56
4.34	DTA thermogram of γ' - Bi_2MoO_6	4.58
4.35	XRD pattern of γ' - Bi_2MoO_6 quenched from melt	4.61

4.36	Arrhenius plots of γ' -Bi ₂ MoO ₆	4.63
4.37	Arrhenius plots of two different pellets of γ' -Bi ₂ MoO ₆	4.64
4.38	Arrhenius plots of γ' -Bi ₂ MoO ₆ (2 nd pellet)	4.65
4.39	Arrhenius plots of γ' -Bi ₂ MoO ₆ sintered at different temperatures	4.66
4.40	Arrhenius plots of γ' -Bi ₂ MoO ₆ pre-sintered at 928°C	4.67
4.41	Complex plane plots of γ' -Bi ₂ MoO ₆ at 550°C: (a) 1 st heating cycle and (b) selected cooling cycles	4.69
4.42	Combined spectroscopic plots of M [∞] and Z [∞] of γ' -Bi ₂ MoO ₆ at 550°C (a) 1 st heating cycle and (b) 4 th cooling cycle	4.70
4.43	Complex plane plot of γ' -Bi ₂ MoO ₆ (pellet sintered at 900°C) at 500°C	4.73
4.44	Complex plane plots of γ' -Bi ₂ MoO ₆ (sintered at 900°C) at high temperatures	4.74
4.45	Arrhenius plots of γ' -Bi ₂ MoO ₆ in two different atmospheres	4.75
4.46	Arrhenius plots of γ' -Bi ₂ MoO ₆ sintered in different environments	4.77
4.47	Isothermal conductivity at 600°C of γ' -Bi ₂ MoO ₆ in different atmospheres	4.78
4.48	SEM micrographs of γ' -Bi ₂ MoO ₆ sintered at (a) 800°C, (b) 850°C, (c) 900°C and (d) after 11 cycles of conductivity measurements	4.79
4.49	Modulus plots of γ' -Bi ₂ MoO ₆ at various temperatures	4.82
4.50	Plots of (a) capacitance and (b) permittivity at Z [∞] _{max} against temperature for data obtained in the 11 th cooling cycle of γ' -Bi ₂ MoO ₆ (1 st pellet)	4.83
4.51	XRD pattern of γ -Bi ₂ MoO ₆	4.86
4.52	Comparison of XRD pattern with JCPDS using μ PDSM: (a) γ -Bi ₂ MoO ₆ and (b) JCPDS card number 21-0102	4.87
4.53	XRD patterns of γ -Bi ₂ Mo _{1-x} M [*] _x O ₈ prepared at 530°C: (a) M [*] =Nb, (b) M [*] =Ta, (c) M [*] =V and (d) M [*] =Cu	4.89

4.54	XRD patterns of γ - $\text{Bi}_2\text{Mo}_{1-x}\text{M}^*_x\text{O}_6$ prepared at 620°C: (a) $\text{M}^*=\text{Nb}$, (b) $\text{M}^*=\text{Ta}$, (c) $\text{M}^*=\text{V}$ and (d) $\text{M}^*=\text{Cu}$	4.90
4.55	IR spectrum of γ - Bi_2MoO_6 showing (a) the whole spectrum and (b) the far IR region	4.91
4.56	DTA thermogram of γ - Bi_2MoO_6	4.93
4.57	Complex plane plots of γ - Bi_2MoO_6 at (a) 375°C, (b) 500°C and (c) 625°C	4.95
4.58	Arrhenius plots of γ - Bi_2MoO_6	4.96
4.59	Spectroscopic plots of γ - Bi_2MoO_6 at (a) 350°C and (b) 450°C	4.98
4.60	Modulus plots of γ - Bi_2MoO_6 at various temperatures (a) 1 st heating cycle and (b) 2 nd heating cycle	4.101
4.61	XRD patterns of γ - $\text{Bi}_2\text{W}_{1-x}\text{Mo}_x\text{O}_6$ prepared at 530 – 710°C	4.102
4.62	XRD patterns of $\text{Bi}_2\text{W}_{1-x}\text{Mo}_x\text{O}_6$ (prepared at 800°C): $x =$ (a) 0, (b) 0.05, (c) 0.10, (d) 0.20, (e) 0.35, (f) 0.40, (g) 0.45 and (h) 0.50	4.104
4.63	XRD patterns of γ' - Bi_2MoO_6 solid solutions, γ' - $\text{Bi}_2\text{Mo}_x\text{W}_{1-x}\text{O}_6$ prepared at 800°C where (a) $x=0.90$, (b) $x=0.95$ and (c) $x=1$	4.105
4.64	XRD patterns of $\text{Bi}_2\text{W}_{1-x}\text{Mo}_x\text{O}_6$ prepared at 800°C: (a) $x=0$, (b) $x=0.60$, (c) $x=0.70$, (d) $x=0.80$, (e) $x=0.85$, (f) $x=1$ and (g) γ - Bi_2MoO_6	4.106
4.65	IR spectra of γ - $\text{Bi}_2\text{W}_{1-x}\text{Mo}_x\text{O}_6$ solid solutions prepared at 530 - 710°C: (a) $x=0$, (b) $x=0.1$, (c) $x=0.3$, (d) $x=0.5$, (e) $x=0.7$, (f) $x=0.9$ and (g) $x=1$	4.108
4.66	IR spectra of $\text{Bi}_2\text{W}_{1-x}\text{Mo}_x\text{O}_6$ solid solutions prepared at 800°C: (a) $x=0$, (b) $x=0.10$, (c) $x=0.20$, (d) $x=0.35$, (e) $x=0.50$ and (f) γ - Bi_2MoO_6	4.109
4.67	IR spectra of γ' - $\text{Bi}_2\text{Mo}_x\text{W}_{1-x}\text{O}_6$ solid solutions prepared at 800°C: (a) $x=1$, (b) $x=0.95$ and (c) $x=0.90$	4.110
4.68	XRD patterns of melted and quenched $\text{Bi}_2\text{W}_x\text{Mo}_{1-x}\text{O}_6$: (a) $x=0$, (b) $x=0.2$, (c) $x=0.4$, (d) $x=0.5$, (e) $x=0.7$, (f) $x=0.8$, (g) $x=0.9$ (h) $x=1$ and (i) unmelted γ' - Bi_2MoO_6	4.113

4.69a	DTA thermograms of γ - $\text{Bi}_2\text{W}_{1-x}\text{Mo}_x\text{O}_6$: (a) $x=0$, (b) $x=0.10$, (c) $x=0.20$, (d) $x=0.40$ and (d) $x=0.50$	4.114
4.69b	DTA thermograms of γ - $\text{Bi}_2\text{W}_{1-x}\text{Mo}_x\text{O}_6$: (f) $x=0.60$, (g) $x=0.80$, (h) $x=0.90$, (i) $x=0.95$ and (j) $x=1$	4.115
4.70	Compositional dependance of phase transition temperatures	4.118
4.71	Phase diagram of Bi_2WO_6 – Bi_2MoO_6 system	4.120
4.72	Arrhenius plots of γ - Bi_2WO_6 (prepared at 710°C)	4.121
4.73	Arrhenius plots of γ - $\text{Bi}_2\text{W}_{0.90}\text{Mo}_{0.10}\text{O}_6$	4.122
4.74	Arrhenius plots of γ - $\text{Bi}_2\text{W}_{0.70}\text{Mo}_{0.30}\text{O}_6$	4.123
4.75	Arrhenius plots of γ - $\text{Bi}_2\text{W}_{0.50}\text{Mo}_{0.50}\text{O}_6$	4.124
4.76	Complex plane plots at 400°C of Bi_2WO_6 (prepared at 710°C) sintered at (a) 710°C and (b) 800°C	4.125
4.77	Spectroscopic plots at 400°C of Bi_2WO_6 (prepared at 710°C) sintered at (a) 710°C and (b) 800°C	4.126
4.78	SEM micrographs of Bi_2WO_6 prepared and sintered at (a) 710°C and (b) 800°C	4.128
4.79	Arrhenius plots of γ - $\text{Bi}_2\text{W}_{0.30}\text{Mo}_{0.70}\text{O}_6$	4.129
4.80	Arrhenius plots of γ - $\text{Bi}_2\text{W}_{0.20}\text{Mo}_{0.80}\text{O}_6$	4.130
4.81	Arrhenius plots of γ - $\text{Bi}_2\text{W}_{0.10}\text{Mo}_{0.90}\text{O}_6$	4.131
4.82	Arrhenius plots of γ - $\text{Bi}_2\text{W}_{0.05}\text{Mo}_{0.95}\text{O}_6$	4.132
4.83	Arrhenius plots of $\text{Bi}_2\text{W}_{1-x}\text{Mo}_x\text{O}_6$ solid solutions	4.134
4.84	Isothermal conductivity of $\text{Bi}_2\text{W}_{1-x}\text{Mo}_x\text{O}_6$	4.135
4.85	Arrhenius plots of γ' - $\text{Bi}_2\text{Mo}_x\text{W}_{1-x}\text{O}_6$ solid solutions	4.136

LIST OF ABBREVIATIONS

ac	alternating current
BIMEVOX	bismuth metal vanadium oxide
dc	direct current
DTA	differential thermal analysis
EMF	electromotive force
EPMA	electron probe microanalysis
FT-IR	Fourier-transform infrared
JCPDS	Joint Committee on Powder Diffraction Standards
μ PDSM	micro Powder Diffraction Search/Match
OFN	oxygen free nitrogen
SEM	scanning electron microscope
SOFC	solid oxide fuel cell
TGA	thermogravimetric analysis
XRD	X-ray diffraction
YSZ	yttria stabilised zirconia
A	area
a, b, c	cell parameters
β	angle between a and c
C	capacitance
C_b	bulk capacitance
C_{gb}	grain boundary capacitance
D	diffusion coefficient
e	elementary charge

ϵ_0	permittivity of free space
ϵ	permittivity
ϵ'	relative permittivity
E	electric field
E_a	activation energy
f	frequency
I	current
k	force constant
l	length
μ	reduced mass
μ_{ion}	mobility of ions
M^*	dopant introduced
M^*	complex electric modulus
M'	real part of electric modulus
M''	imaginary part of electric modulus
N_{ion}	number of ions
ω	angular frequency
P''_{O_2}	partial pressure of O ₂ of reference material
P'_{O_2}	partial pressure of O ₂ of sample
R	resistance
ρ	resistivity
σ	conductivity

τ	relaxation time
T	temperature
$\tilde{\nu}$	wavenumber
X	reactance
Z^*	impedance
Z'	real part of impedance
Z''	imaginary part of impedance

CHAPTER 1

INTRODUCTION

1.1 Solid Electrolytes and Oxide Ion Conductors

Electrical conduction occurs by the long-range diffusion of either electrons or ions. Usually, conduction by one or the other type of charge carrier predominates but in some inorganic materials both ionic and electronic conduction are significant.

Migration of ions at normal temperatures does not occur to any appreciable extent in most ionic and covalent bonded solids such as oxides and halides. For example, NaCl is an insulator at room temperature with a conductivity of only $\sim 10^{-15} \text{ S cm}^{-1}$.

The idea that ions can diffuse as rapidly in a solid as in an aqueous solution or in a molten salt may seem astonishing. However, since the 1960s, a variety of solids that include crystalline compounds, glasses, polymers and composite materials with exceptionally high ionic conductivities have been discovered. Many of these materials have been synthesised and studied. These include materials where the conduction species are anions (eg. F^- and O^{2-}) or cations (e.g. H^+ , Li^+ , Na^+ , Cu^+ , Ag^+). A variety of names have been given for these materials including solid electrolytes, superionic conductors, and fast-ion conductors. ‘Solid electrolytes’ arguably provides the least misleading and broadest description for this class of materials. Such materials often have rather special crystal structures in that there are open tunnels or layers through which the mobile ions may move.

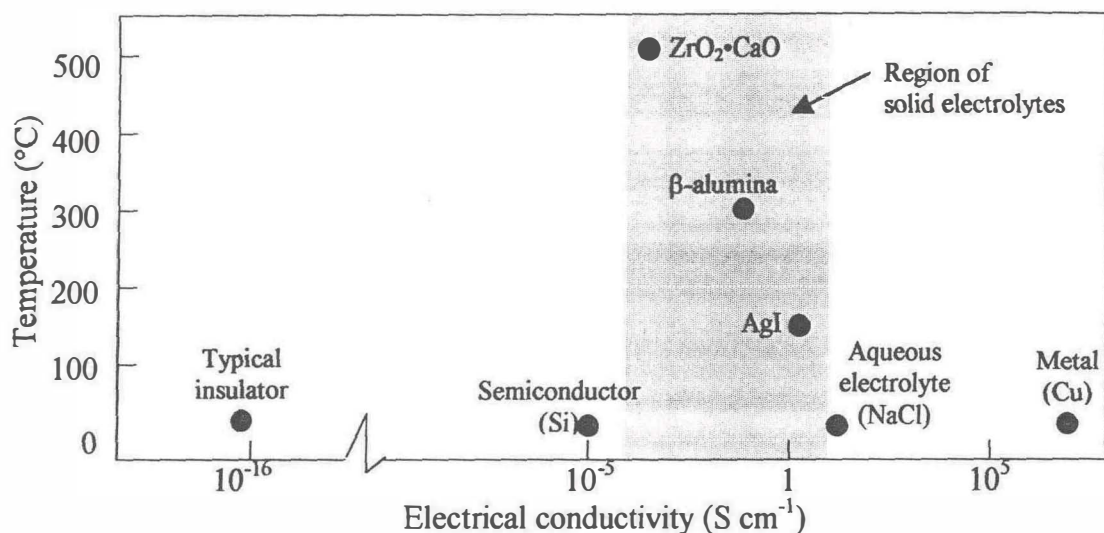


Figure 1.1: Electrical conductivities of selected common substances and representative solid electrolytes (Greenblatt, 1994)

In Figure 1.1, the electrical conductivities of several common substances and representative solid electrolytes are shown at the temperatures where the materials have potential application. The solid electrolytes have conductivities that fall between those of a typical semiconductor, silicon and a typical aqueous electrolyte, sodium chloride.

There has been active research in the area of fast-ion transport in solids in recent years, partly because of the many potential technological applications of solid electrolytes. These applications include high-energy-density batteries, fuel cells, sensors, electrochromic materials for both optical display and 'smart window' devices, low-cost electrolysis of water and selective atomic filters. Devices using solid electrolytes are already available commercially: oxygen detectors for automotive pollution-control systems employ solid O^{2-} conductors and solid-state batteries using Li^+ conducting solid electrolytes are employed in heart pacemakers.